Viability of a Frictionless Bearing with Permanent Magnets and HTS Bulks

A.J. Arsénio, M.V. Carvalho, C. Cardeira, P.J. Costa Branco
IDMEC, Instituto Superior Técnico, Universidade de Lisboa, Portugal

R. Melício
IDMEC, Instituto Superior Técnico, Universidade de Lisboa
Departamento de Física, Escola de Ciências e Tecnologia
Universidade de Évora, Portugal

***Abstract*—This paper studies the technical viability of a frictionless rotating bearing model comprising one inner rotor part with discontinuous rings with permanent magnets and one outer stator part with discontinuous rings with high temperature superconducting bulks, distributed on a geometric arrangement that guarantees enhanced levitating and guidance forces using the zero field cooling technique. Extensive Finite Element model simulations were carried out to estimate levitation and guidance forces depending on the air gap dimensions. Eccentricity and axial displacement of the rotor are estimated depending on the external radial and axial forces applied to the rotor. Finally, the proposed design of a viable and feasible frictionless bearing prototype is foreseen.**

Keywords—Frictionless rotating bearing; levitation and guidance forces; zero field cooling; permanent magnets; HTS bulks.

I. INTRODUCTION

Superconductivity is the phenomenon of certain materials exhibiting zero electrical resistance and the expulsion of magnetic fields under specific temperature, magnetic field and current conditions. Each superconducting material has an absolute critical temperature T_C above which it loses its superconducting properties [1]. In 1911 superconductivity was first observed by the Physicist Heike Kamerlingh Onnes [2]. He noticed that when the mercury (Hg) is cooled to the boiling point of helium (He) which is 4.2 K, the electrical resistivity of mercury is almost zero. In 1913 it was discovered that lead (Pb) has almost zero resistivity at absolute temperatures below 7 K. In 1933 the researchers Walther Meissner and Robert Ochsenfeld noticed that superconductors expelled applied magnetic fields, a phenomenon that has come to be known as the Meissner effect [3]. In 1935, the brothers Fritz London and Heinz London showed that the Meissner effect was a consequence of minimization of the electromagnetic free energy carried by superconducting current. In 1950 Lev Landau and Vitaly Ginzburg postulated the Ginzburg-Landau theory of superconductivity basing on which it was possible to first explain the behavior of type II superconductors [3].

The complete microscopic theory of superconductivity was finally proposed in 1957 by John Bardeen, Leon N. Cooper, and Robert Schrieffer, known as the BCS theory. The BCS theory explains the superconducting current as a superfluid of Cooper pairs, pairs of electrons interacting through the exchange of phonons. The main peak of discoveries took place between 1986 and 1987, when high temperature superconductors (HTS) with critical absolute temperatures above 30 K started to be discovered. In 1987, the Chu's group and Kitazawa's group jointly announced and published the discovery of Yttrium-Barium-Copper-Oxide, i.e., YBa2Cu3O7 (YBCO) with critical temperature 92 ºK, as type II superconductor. The discovery of the YBCO was an important achievement because liquid nitrogen could now be used for cooling instead of the expensive liquid helium.

Type I superconductors are characterized by only one state of superconductivity (Meissner state), presenting diamagnetic properties for magnetic flux densities below a critical value B_C. Type II superconductors are characterized by having two states of superconducting operation, depending on the value of the applied magnetics flux density [3]. On the first state (Meissner state) repeal completely magnetic fields below a critical magnetic flux density B_{C1}. On the second state (Vortex state) trap magnetic fields between B_{C1} and an upper critical value of magnetic flux density B_{C2}. For fluxes between B_{C1} and B_{C2}, the magnetic field starts to cross through defect granularities forming magnetic field tunnels in the composite. The current vortexes are induced around these magnetic field tunnels. Because of the almost null resistivity below the critical temperature T_C the induced current vortexes remain for very long periods [3]. Fig. 1 shows typical phase diagrams, giving the dependence of the magnetic flux density critical values on the superconductor temperature, for type I and type II superconductors.

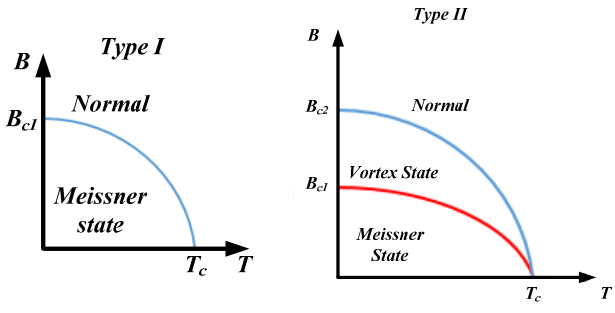

Figure 1. Phase diagrams of type I and type II superconductors.

The superconductor materials lose also the superconducting properties if crossed by electrical current densities higher than a characteristic critical current density J_C [3].

When type II superconductor bulks are cooled in presence of a magnetic field between B_{C1} and B_{C2} (Vortex state), known as the field cooling (FC) technique, they trap and memorize that magnetic field. After field cooled they perform as permanent magnets (PMs), generating a magnetic field equal to the trapped field. Magnetic forces exist when they are located in the middle of an existing magnetic field different to the trapped field, being repealed to a position where the existing magnetic field almost equals the trapped field [4,5].

In the case that superconductor bulks are cooled with the presence of magnetic fields below B_{C1} (Meissner state), they become diamagnetic repealing those magnetic fields. The zero field cooling (ZFC) technique consists in cooling a superconductor in the absence of magnetic fields. When a zero field cooled superconductor bulk is positioned in the middle of an existing magnetic field it is repealed to a position where the magnetic flux is nearly zero [4,5]. Hence, levitation systems can be ZFC or FC [6,7].

Some of the existing levitation systems use permanent magnets on one part and type II superconductor bulks on the other part and are used as frictionless rotating bearings. The frictionless rotating bearing can be sub-divided into horizontal axis rotating systems, in which the levitation forces are radial and the vertical axis rotating systems, in which the levitation forces are axial to a vertical axis [8-11].

Some horizontal or vertical axis rotating systems based on levitation forces are shown in Table I.

TABLE I. ROTATING SYSTEMS BASED ON LEVITATION FORCES

Axis	Use	Angular speed (rpm)	Stator	Rotor	Reference
Horizontal	Flyweel	40000	NdFeB PM	YBCO bulks	[8]
Vertical	Flyweel	4000	YBCO bulks	NdFeB PM	[9]
Horizontal	HTS motor	1500	YBCO	NdFeB PM	[10]
Horizontal	Flyweel	15860	YBCO	PM rings	[11]

In [12,13] the frictionless superconductor magnetic bearing (SMB) systems studied were designed to levitate based on the FC technique. The FC technique implies significant hysteresis losses due to the magnetic flux trapping. In [14] it is proposed a linear electromagnetic launcher with a propulsion forces using Meissner effect based on ZFC technique. In [7,15] it is proposed a linear HTS magnetic levitation system based on the ZFC technique with guidance. The guidance is obtained by an adequate distribution of existing magnetic fields, generated by specific array configurations of multi-pole permanent magnets.

In a SMB, the symmetric radial magnetic levitation forces, i.e., levitation forces and the symmetric axial magnetic guidance forces, i.e., guidance forces are important. Levitation forces are the equally distributed radial magnetic forces that keep the axis of the rotor aligned with the stator axis in the absence of gravity or external radial forces. Guidance forces are the existing magnetic axial forces that in absence of axially external forces keep the superconductor bulks positioned between the magnets [16]. The resultant of the levitation forces integrated along the rotor periphery is zero [16]. The resultant of the guidance forces integrated along the rotor axis should be zero [16].

The main contribution of this paper is the viability analysis of a new ZFC based SMB made of HTS bulks and PMs. A specified geometry is proposed and simulated, analyzing if a real prototype of a ZFC SMB can be foreseen.

This paper is organized as follows: Section II presents the modeling of the frictionless rotating bearing prototype. Section III presents the proposed design. Section IV shows the case study. Finally in Section V some conclusions are drawn.

II. MODELING

The cylindrical geometry of the frictionless rotating bearing model studied is based on the linear HTS magnetic levitation system using a ZFC technique presented in [7,15]. Repulsion of magnetic fields can be modeled considering a relative permeability lower than the unit $\mu_r < 1$ for HTS bulks.

The magnetization M of the PMs is given by:

$$M = B_r / \mu_0 \ . \tag{1}$$

where B_r is the permanent magnet remainder magnetic flux density, μ_0 is the vacuum magnetic permeability.

The type II superconductors, in the case of ZFC technique, create diamagnetic fields such that, the normal component of the resultant magnetic field on the boundary of the superconductor surfaces becomes almost zero [7]. The diamagnetic field is created by a superficial peripheral current density on the superconductor that contributes for the levitation forces [7]. Hence, a specific volume crossed by a specific current density under the influence of a magnetic field suffers a volume force density $\bar{f}$ [17] is given by:

$$\bar{f} = \bar{J} \times \bar{B} \ . \tag{2}$$

$$\bar{f} = \mu(\bar{\nabla} \times \bar{H}) \times \bar{H} = \mu(\bar{\nabla} \bullet \bar{H})\bar{H} - \frac{\mu}{2}\bar{\nabla}(\bar{H} \times \bar{H}) \cdot \tag{3}$$

where $\bar{J}$ is the current density in the superconductor, $\bar{B}$ is the magnetic flux density, μ is the medium magnetic permeability and $\bar{H}$ is the magnetic field.

The volume force density can be decomposed in Cartesian coordinates system [17] given by:

$$f_m = \frac{\partial}{\partial n}(\mu H_n H_m - \frac{\mu}{2}\delta_{mn}|H|^2) \quad ; \quad \delta_{mn} = \begin{cases} 0 & m \neq n \\ 1 & m = n \end{cases}. \qquad (4)$$

where f_m is the volume strength density component, $m,n = (x,y,z)$ depending on the considered component, H_n and H_m are the magnetic field components and δ_{mn} is a Kronecker delta.

The component f_m of the volume force density is the gradient in n direction of the Maxwell stress tensor component T_{mn} depending on the magnetic field components H_n and H_m [17]. T_{mn} is given by:

$$T_{mn} = \mu H_n H_m - \frac{\mu}{2}\delta_{mn}|H|^2 . \qquad (5)$$

Consider a cube or rectangular block with one of the six surfaces parallel to the xy plan. Using ZFC technique, the value of the magnetic field normal component to this surface should be zero $H_z = 0$. The normal component of the Maxwell stress tensor to this surface T_{zz} [17] is given by:

$$T_{zz} = -\frac{\mu}{2}(H_x^2 + H_y^2) . \qquad (6)$$

Consider n and t as normal and tangential components of the Maxwell stress tensor. (6) can be rewritten, as given by:

$$T_n = -\frac{\mu}{2}|H_t|^2 . \qquad (7)$$

where T_n is the Maxwell stress tensor normal component and H_t is the magnetic field tangential component to the surface parallel to the xy plane.

The levitation and guidance forces can be calculated by integrating the Maxwell stress tensor along the superconductor surfaces.

The levitation forces F_{Lev} along z axis [17] are given by:

$$|F_{Lev}| = \frac{A}{\mu}\frac{|B_t|^2}{2} . \qquad (8)$$

where A is the surface parallel to the xy plan and B_t is the magnetic flux density tangential component.

III. Proposed Design

Considering that the ZFC SMB will be composed by a static part (stator) and a rotating part (rotor), the rotor is the part that should levitate. Hence, the proposed design of the frictionless rotating SMB model has an inner rotor part including the trails of PMs and an outer stator part the discontinuous lines of HTS bulks. The outer stator part contains 2 discontinuous rings of equally spaced of YBCO HTS bulks. An alternative approach using PMs and HTS rings instead of bulks was discarded for economic reasons. Actual rings have to be made with specific geometry and dimensions, whereas generic bulks are much cheaper and easier to obtain.

The inner rotor part contains 3 discontinuous rings with 5 equally spaced NdFeB permanent magnets.

All PMs belonging to the same discontinuous ring, are magnetized with concordant poles towards the axis. The 3 inner discontinuous rings of PMs are magnetized in alternate North-South-North way, such as the 2 border rings of magnets have concordant polarizations and the middle ring of magnets opposite polarization. The perspective view of the frictionless SMB with spatial distribution of PMs and of HTS bulks is shown in Fig. 2.

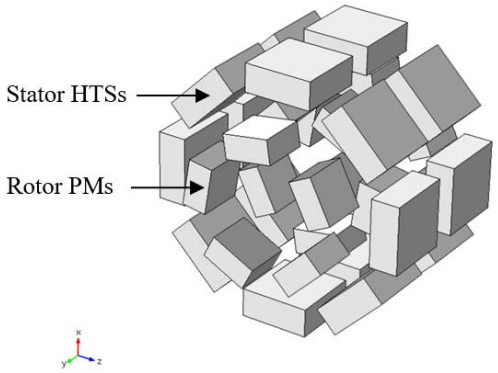

Figure 2. Perspective view: spatial distribution of PMs and HTSs bulks.

The projection views of the frictionless SMB geometry (and dimensions) are shown in Fig. 3.

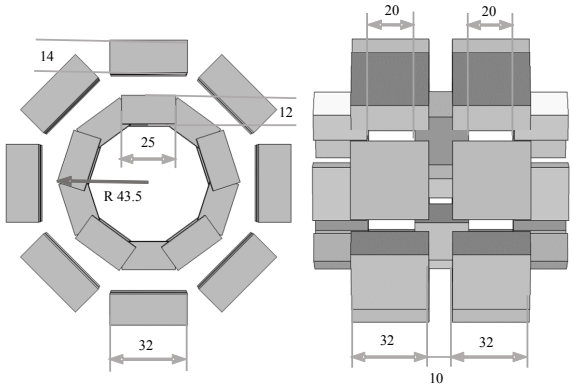

Figure 3. Projection view: spatial distribution of PMs and of HTSs bulks.

The discontinuous rings of PMs and the discontinuous rings of HTS bulks are interposed in such a way to provide guidance forces.

IV. Case Study

Several case studies were analyzed. For all the case studies, calculations were performed by simulation using a finite element modeling (FEM). The PMs are made of NdFeB material and the HTS bulks are made of YBCO material. Each

PM has rectangular form with dimensions 25x25x12 mm and a mass of 0.06 kg. Each HTS has rectangular form with dimensions 32x32x14 mm and a mass of 0.09 kg. For the simulations both FC and ZFC techniques are analyzed. The assumed value of the permanent magnet remainder magnetic flux density is $B_r = 1.2\ T$ [10]. For ZFC, the assumed relative magnetic permeability for the HTS bulks is $\mu_r = 0.2$ [4,5,18].

A. Case 1- levitation forces between one PM and one HTS

This case study simulates and evaluates the levitation forces, namely the repulsion forces between one PM and one HTS. For the simulation it is assumed that both the PM and the HTS are horizontally disposed with both centers aligned at a given vertical distance. An example of the simulation showing the ZFC distribution of magnetic flux between the PM and the HTS at 12 mm vertical distance is shown in Fig 4.

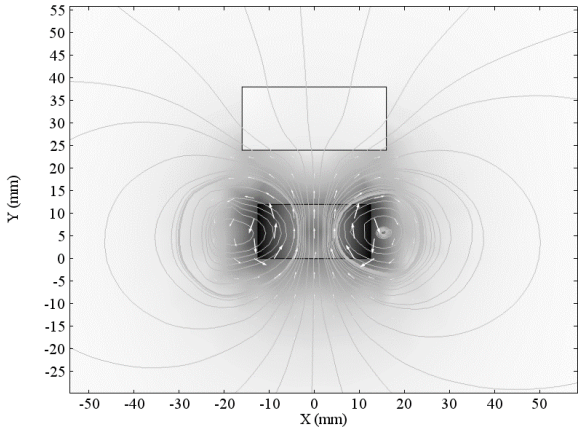

Figure 4. ZFC distribution of magnetic flux at 12 mm vertical distance.

Both ZFC and FC techniques were simulated and compared. Several distances between the upper surface of the PM and the lower surface of the HTS were considered. For FC, the magnetization distances are also taken into account. The ZFC and FC techniques: repulsion forces between a PM and a HTS at several distances is shown in Fig. 5.

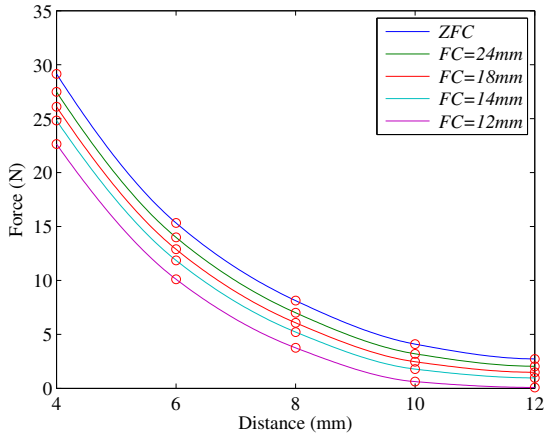

Figure 5. ZFC and FC techniques: repulsion forces between a PM and a HTS at several distances.

Fig. 5 clearly shows that the ZFC repulsion forces between the PM and the HTS at several vertical distances are always higher than FC repulsion forces. Moreover, it shows that when the FC magnetization distances increase, the repulsion forces get closer to ZFC, as expected.

The results obtained for the repulsion forces between the PM and the HTS (Fig. 5) are similar to the ones presented in [4,19].

B. Case 2 - SMB levitation and guidance forces

This case study evaluates the levitation forces and the guidance forces between the PMs and the HTSs for the proposed design of the frictionless rotating SMB. Several air gap distances were considered.

The perspective view of the magnetization directions and contours for the frictionless rotating SMB is represented in Fig 6.

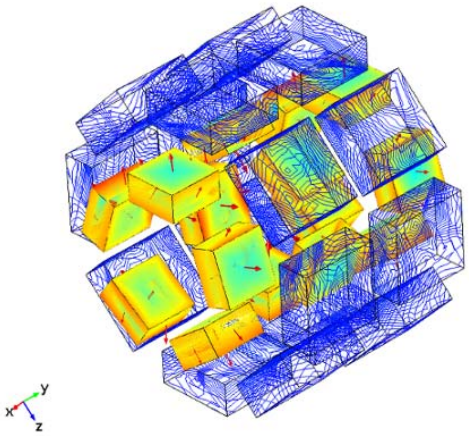

Figure 6. SMB:perspective view of magnetization directions and contours.

The transversal view of the magnetization directions and contours for the frictionless rotating SMB is shown in Fig. 7.

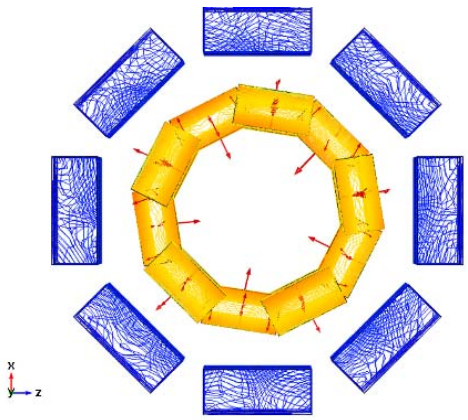

Figure 7. SMB: transversal view of magnetization directions and contours.

The longitudinal view of the magnetic flux density lines for the frictionless rotating SMB is shown in Fig. 8.

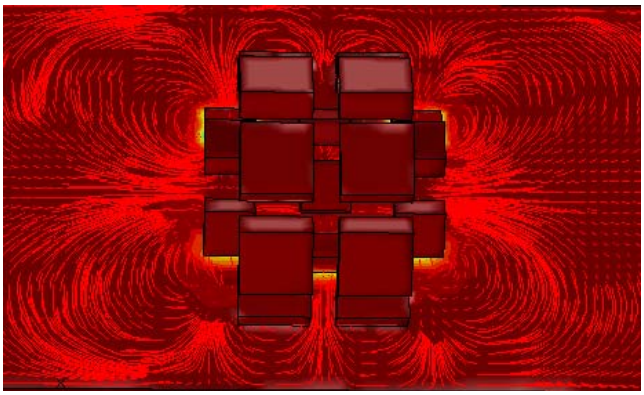

Figure 8. SMB: transversal view of magnetic flux contours.

The arrows (Fig. 6 to Fig. 8) represent the magnetic polarization direction of the PMs.

The levitation forces and the guidance forces versus the air gap size for the frictionless rotating SMB in both ZFC and FC modes are shown in Fig. 9 and Fig. 10. Results for FC are shown for 150% and 200% relation between the cooling distance and operational distance [6]. In this case, the operational distance is equal to the air gap. These figures show that levitation forces and guidance forces decrease when the air gap increases, as expected. Moreover, these figures clearly show that the forces obtained using ZFC technique outperform those obtained by the FC technique.

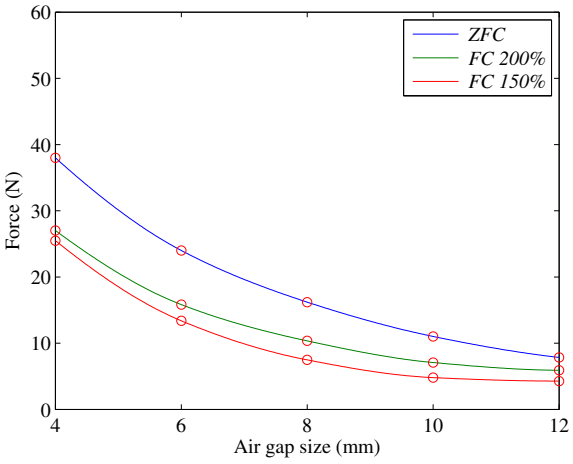

Figure 9. Frictionless SMB: levitation forces.

The total weight of the 15 PM in the rotor is about 8.83 N. The total weight of the 16 bulks in the stator is about 14.12 N. Fig. 8 and Fig. 9 show that for ZFC the levitation and guidance forces are higher than the rotor weight. Hence the SMB seems viable and self-sustainable in both horizontal and vertical positions. More details are shown in Tables II and Table III.

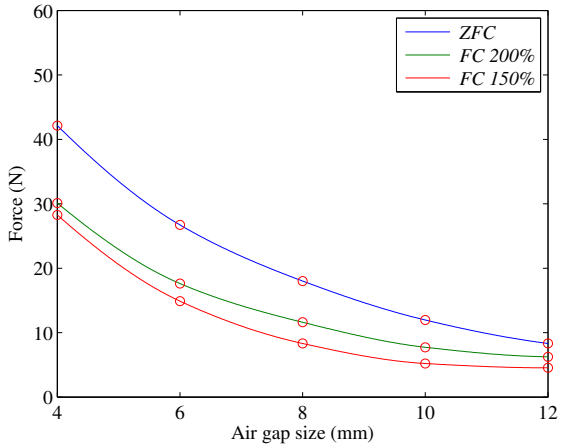

Figure 10. Frictionless SMB: guidance forces.

The axial forces impose a specific translation displacement of the rotor axis from the equilibrium position. The axial forces for a translation between 2 mm and 8 mm and an air gap of 4 mm and 10 mm are shown in Table II.

TABLE II. AXIAL FORCES FOR A TRANSLATION

Air gap 4 mm				
Translation	**2 (mm)**	**4 (mm)**	**6 (mm)**	**8 (mm)**
Axial forces (N)	12.74	24.87	35.66	42.44
Air gap 10 mm				
Axial forces (N)	3.45	6.81	9.18	10.84

As expected these forces are much higher for an air gap of 4 mm.

The radial forces impose a specific eccentricity of the rotor axis from the stator axis. The radial forces between 2 mm and 8 mm and an air gap of 10 mm are shown in Table III.

TABLE III. RADIAL FORCES AND ROTOR EXCENTRICITY

Air gap 10 mm				
Eccentricity	**2 (mm)**	**4 (mm)**	**6 (mm)**	**8 (mm)**
Radial forces (N)	6.19	12.79	24.11	39.46

As expected, higher applied external radial forces lead to higher rotor eccentricity. From the above discussion it is possible to conclude that a 10 mm airgap will lead to a self-sustainable frictionless SMB.

The frictionless rotating SMB proposed design foreseen is shown in Fig. 10.

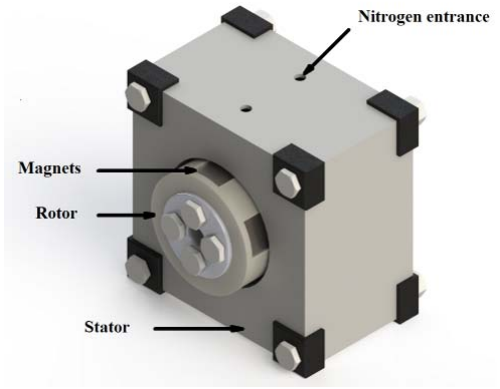

Figure 11. Frictionless rotating SMB foreseen design.

The resulting frictionless rotating SMB geometry and air gap dimensions are adequate to create levitation and guidance forces showing that the SMB is viable and feasible.

V. CONCLUSIONS

In this paper the analysis of levitation and guidance forces for a frictionless rotating bearing model with discontinuous rings of superconductors, based on a zero field cooling technique, was performed. From the obtained results, it was concluded that ZFC over performs FC technique and that there is an upper air gap size limit to support the rotor weight.

Accordingly, the frictionless rotating bearing model is technical viable with the studied geometry based on a zero field cooling technique. The rotor radial eccentricity and rotor axial translation displacements depend on applied external radial and axial stresses. The air gap dimensions should be chosen according to the axial and radial stress that the rotor vein should support. Future work should be carried out, in order to evaluate the increase in levitation and guidance forces for an equivalent but more expensive model with same rotor geometry, but with continuous rings of superconductors and the cost effectiveness of such a modified frictionless bearing model.

ACKNOWLEDGMENT

This work is funded by support of fellowship EMS/50022 granted by IDMEC/LAETA to A.J. Arsénio, as researcher in this R&D Institution and as PhD Student at Instituto Superior Técnico, Universidade de Lisboa, Portugal; and by Portuguese Funds through the Foundation for Science and Technology-FCT under the project LAETA 2015 - 2020, reference UID/EMS/50022/2013.

REFERENCES

[1] J. Evetts; University of Cambridge, England, "The characterization of superconducting materials-conflicts and correlations," IEEE Trans. on Magnetics, vol. 19(3), pp. 1109-1119, May 1983.

[2] C.W. Chu, "High-temperature superconducting materials: a decade of impressive advancement of Tc," IEEE Transactions on Applied Superconductivity, vol. 7(2), pp. 80-89, June 1997.

[3] L.D. Landau, and E.M. Lifshitz, "*Electrodynamics of continuous media"*, 2nd Edition, Oxford, UK: Pergamon Press, 1968.

[4] B. Painho, J.A. Dente, and P.J. Costa Branco, "Superconductor losses and damping effects under zero field cooling and field cooling conditions in a HTSC-magnet levitation system," Jornal of Superconductivity and Novel Magnetism, vol. 24(1), pp. 927–937, January 2011.

[5] J. Arnaud, and P.J. Costa Branco, "Electrothermal characteristics of YBCO bulk magnets deep in LN_2: a preliminary analysis for its use as excitation system of low-speed synchronous generators," IEEE Transactions on Applied Superconductivity. vol. 26(3), April 2016.

[6] J. Zheng, Z. Deng, L. Wang, L. Liu, Y. Zhang, S. Wang, and J. Wang, "Stability of the maglev vehicle model using bulk high T_c superconductors at low speed," IEEE Transactions on Applied Superconductivity, vol. 17(2), pp. 2103-2106, June 2007.

[7] P.J. Costa Branco, and J.A. Dente, "Design and experiment of a new maglev design using zero-field-cooled YBCO superconductors," IEEE Transactions on Industrial Electronics, vol. 59(11), pp. 4120-4127, November 2012.

[8] T.H. Sung, S.C. Han, J.S. Lee, N.H. Jeong, S.D. Hwang, and S.K. Choi, "Designs and analyses of flywheel energy storage systems using high-T_c superconductor bearings," Cryogenics, vol. 42, pp. 357-362, 2002.

[9] Y.H. Han, B.J. Park, S.Y. Jung, and S.C. Han, "Study of superconductor bearings for a 35 kWh superconductor flywheel energy storage system," Physica C: Superconductivity, vol. 483, pp. 156-161, 2012.

[10] P. Kummeth, W. Nick, and H.-W. Neumueller, "Progress in development of high capacity magnetic HTS bearings," Physica C: Superconductivity, vol. 426-431, pp. 739-745, October 2005.

[11] T. Ichihara, K. Matsunaga, M. Kita, I. Hirabayashi, M. Isono, M. Hirose, K. Yoshii, K. Kurihara, O. Saito, S. Saito, M. Murakami, H. Takabayashi, M. Natsumeda and N. Koshizuka, "Fabrication and evaluation of superconducting magnetic bearing for 10 kW h-class flywheel energy storage system", Physica C, vol. 426–431, pp. 752–758, 2005.

[12] P.D. Barba, H. May, M.E. Mognaschi, R. Palka, and A. Savini, "Shape design optimization of the excitation arrangement and superconducting bulks used in magnetic bearings," in Proc. XV International Symposium on Theoretical Engineering, pp. 1-4, June 2009.

[13] M. Sparing, A. Berger, F. Wall, V. Lux, S. Hameister, D. Berger, M. Hossain, A. Abdkader, G. Fuchs, C. Cherif, and L. Schultz, "Dynamics of rotating superconducting magnetic bearings in ring spinning," IEEE Transactions on Applied Superconductivity, vol. 26(3), pp. 1-4, April 2016.

[14] P.J. Costa Branco, R. Almeida, and J.A. Dente, "On using Meissner effect to conceive a new linear electromagnetic launcher by zero-field-cooling YBCO bulk superconductors," IEEE Transactions on Industrial Electronics, vol. 61(11), pp. 5894-5902, November 2014.

[15] J. Fernandes, I. Montes, R. Sousa, C. Cardeira, and P.J. Costa Branco, "Superconductor joule losses in a zero-field-cooled (ZFC) maglev vehicle," IEEE Transactions on Applied Superconductivity, vol. PP(90), pp. 1-7, February 2016.

[16] F. Freschi and M. Repetto, "Natural Choice of Integration Surface for Maxwell Stress Tensor", IEEE Transactions on Magnetics, vol. 49, no. 5, pp.1717-1720, May 2013.

[17] François Henrotte, Kay Hameyer, "Computation of electromagnetic force densities: Maxwell stress tensor vs. virtual work principle", Journal of Computational and Applied Mathematics vol. 168, pp. 235–243, 2004.

[18] H. Fujishiro, T. Naito, and D. Furuta, "Analysis of temperature and magnetic field distribution in superconducting bulk during pulsed field magnetization," IEEE Transactions on Applied Superconductivity, vol. 21(3), pp. 2723-2726, June 2011.

[19] J.S. Wang, S.Y. Wang, Z.Y. Ren, M. Zhu, H. Jiang, and Q.X. Tang, "Levitation force of a YBaCuO bulk high temperature superconductor over a NdFeB guideway," IEEE Transactions on Applied Superconductivity, vol. 11, pp. 1801-1804, 2001.